AAS 18-289

DISPOSAL TRAJECTORIES FROM NEAR RECTILINEAR HALO ORBITS

Kenza K. Boudad*, Diane C. Davis†, and Kathleen C. Howell‡

After completion of a resupply mission to NASA's proposed Lunar Orbital Platform - Gateway, safe disposal of the Logistics Module is required. One potential option is disposal to heliocentric space. This investigation includes an exploration of the trajectory escape dynamics from an Earth-Moon Near Rectilinear Halo Orbit (NRHO) and applies these insights to the design of a low-cost heliocentric Logistics Module disposal option. The effects of the solar gravitational perturbations are assessed in both the bicircular restricted 4-body problem and in an ephemeris force model.

INTRODUCTION

The proposed Lunar Orbital Platform - Gateway is the current framework for the NASA development of a space facility near the Moon with an option to return to the lunar surface.[1,2] From a baseline trajectory concept in a Near Rectilinear Halo Orbit (NRHO), the Gateway is intended to serve as a proving ground for deep space technologies and as a staging location for missions beyond cislunar space. The Orion spacecraft is planned to transport crew to the Gateway, with resupply missions executed by one or more Logistics Modules (LM).[1] After completion of a resupply mission, safe disposal of the LM is required, and one potential option is disposal to heliocentric space.

The NRHO and a sample disposal trajectory appear in Figure 1. The current investigation includes exploration of the trajectory escape dynamics from an NRHO and leverages these insights to the design of a heliocentric LM disposal option. The perturbing effects of the Sun on the LM orbit as it escapes from the Earth-Moon NRHO are critical to any heliocentric disposal design. The solar gravitational perturbations are assessed in both the Bicircular Restricted 4-Body Problem (BCR4BP) and an ephemeris force model. To successfully reach heliocentric space along an escape path, solar orientation (epoch) and energy level are key contributors. To assess their impact, this analysis suggests departure criteria and illustrates the results via sample scenarios.

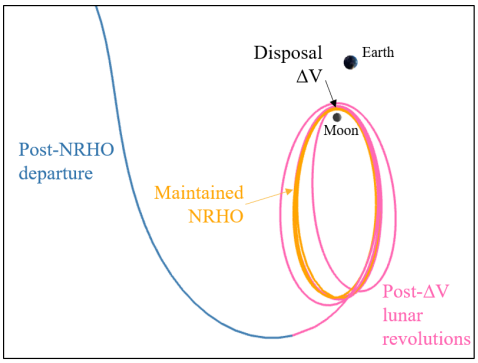

Figure 1: Sample NRHO disposal trajectory as viewed in the Earth-Moon rotating frame.

DYNAMICAL MODELS

In this investigation of a vehicle disposal from an Earth-Moon NRHO, the Bicircular Restricted 4-Body Problem (BCR4BP) and a higher-fidelity ephemeris model serve as the dynamical bases for the analysis.

*Graduate Student, School of Aeronautics and Astronautics, Purdue University, Armstrong Hall of Engineering, 701 W. Stadium Ave., West Lafayette, IN 47907-2045, kboudad@purdue.edu.
†Principal Systems Engineer, a.i.solutions, Inc., 2224 Bay Area Blvd, Houston TX 77058, diane.davis@ai-solutions.com.
‡Hsu Lo Distinguished Professor, School of Aeronautics and Astronautics, Purdue University, Armstrong Hall of Engineering, 701 W. Stadium Ave., West Lafayette, IN 47907-2045, howell@purdue.edu. Fellow AAS; Fellow AIAA

The BCR4BP incorporates the influence of solar gravity on the Earth-Moon-spacecraft three-body system and offers an increase in fidelity over the Circular Restricted 3-Body Problem (CR3BP). A higher-fidelity N-body model, based on ephemeris data, accommodates additional forces and perturbations as modeled in the FreeFlyer software package. Numerical simulations in the ephemeris model are necessary but generally time-consuming and inefficient without sufficient insight into the behavior under the multiple gravitional influences. The use of the BCR4BP therefore avoids increased complexity but captures the most significant influences on the behavior. Suitable disposal trajectories obtained in the BCR4BP are then transitioned to the higher-fidelity ephemeris model.

The Bicircular Restricted Four-Body Problem

The BCR4BP[3] incorporates the gravitational impact of three massives bodies, for instance, the Earth E, the Moon M and the Sun S, on the motion of a spacecraft P. The mass of P is assumed to be negligible in comparison to the masses of the other bodies. Denote the Earth and the Moon as the primary bodies. The Earth and the Moon are assumed to move in circular orbits around their common barycenter B_1 as defined in Figure 2. The Sun and B_1 then move in circular orbits around the E-M-S system barycenter B_2. As apparent in Figure 2, the plane of Earth-Moon primary motion and the Sun orbital plane are not assumed to be coplanar in this model. This BCR4BP model is not coherent since the motions of the primaries and the Sun are not a solution of the general 3BP. Coherent restricted 4-body models have been the subject of other investigations[4,5] but the additional complexity is not necessary for this analysis. In addition to the inertial frame, two rotating frames are defined in Figure 2. An Earth-Moon (E-M) rotating frame is fixed the $\hat{x}$ axis lies along the Earth-Moon line, the $\hat{z}$ axis is aligned with primaries' orbital angular momentum, and the $\hat{y}$ axis completes the right-handed orthonormal set. The solar orbital plane is defined by the inclination i with respect to the Earth-Moon plane and the longitude Ω of the Sun's ascending node along its orbit. The second rotating frame, Sun-B_1 is fixed in the motion of the Sun and B_1, the Earth-Moon barycenter. The $\hat{x}'$ axis is defined along the line joining the Sun to B_1, $\hat{z}'$ is aligned with the Sun and B_1 angular momentum vector, and $\hat{y}'$ completes the right-handed orthornomal set. The differential equations governing motion in the BC4BP are derived by adding the solar gravity influence to the Earth-Moon CR3BP. The Sun angle, θ_S, is the angle between the projection of the rotating $\hat{x}$ axis on the Sun orbital plane and the Sun position vector relative to B_1 and is linearly decreasing: $\theta_S = -\omega_S\, t$ as apparent in Figure 3. The position vector for P, $\bar{x}^{\alpha}_{\beta}$, is expressed as a row vector in the frame α with respect to the basepoint β. The direction cosine matrix that rotates row position vectors from the E-M rotating frame to the Sun-B_1 rotating frame is defined as follows,

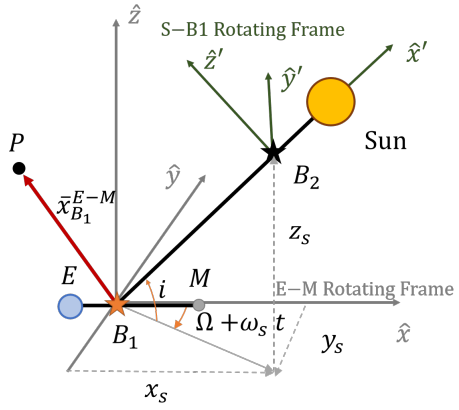

Figure 2: Frames and vectors definitions in the BCR4BP.

$$\bar{x}_{B_1}^{S-B_1\ \text{Rotating}} = \bar{x}_{B_1}^{E-M\ \text{Rotating}}\,\mathbf{A} \tag{1}$$

where

$$\mathbf{A} = \begin{bmatrix} \cos(\theta_S - \Omega - \pi) & -\sin(\theta_S - \Omega - \pi) & 0 \\ \sin(\theta_S - \Omega - \pi) & \cos(\theta_S - \Omega - \pi) & 0 \\ 0 & 0 & 1 \end{bmatrix} \begin{bmatrix} 1 & 0 & 0 \\ 0 & \cos(i) & -\sin(i) \\ 0 & \sin(i) & \cos(i) \end{bmatrix} \begin{bmatrix} \cos(\Omega) & -\sin(\Omega) & 0 \\ \sin(\Omega) & \cos(\Omega) & 0 \\ 0 & 0 & 1 \end{bmatrix} \tag{2}$$

The velocity vector for P is labeled $\dot{\bar{x}}_{B_1}^{E-M\text{Rotating}}$ in the E-M rotating frame, and can be transformed to the velocity vector in the Sun-B_1 rotating frame:

$$\dot{\bar{x}}_{B_1}^{S-B_1\ \text{Rotating}} = \dot{\bar{x}}_{B_1}^{E-M\ \text{Rotating}}\,\mathbf{A} + \bar{x}_{B_1}^{E-M\ \text{Rotating}}\,\dot{\mathbf{A}} \tag{3}$$

where $\dot{\mathbf{A}}$ is the derivative of $\mathbf{A}$ with respect to time. For computational purposes, the states in the BCR4BP are nondimensionalized using characteristic quantities. The characteristic mass m^* is the sum of the masses of Earth and the Moon. The characteristic distance l^* is the distance between the Earth and the Moon

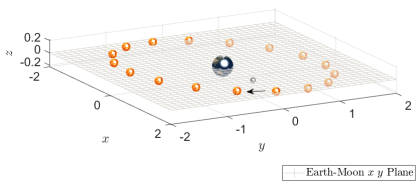

Figure 3: **Sun's orbit (not to scale) as viewed in the Earth-Moon Rotating Frame.**

and is assumed constant. Choosing the nondimensional angular motion of E and M to be equal to one yields the nondimensional characteristic time t^*. The Sun's mass, m_S, its distance from the Earth-Moon barycenter (B_1), a_S, and the solar angular velocity with respect to the Earth-Moon rotating frame, w_S, are nondimensional values defined with the characteristic quantities. The nondimensional mass parameter μ is defined as the mass of the Moon over the characteristic mass, m^*. The equations of motions of the BCR4BP are

$$\begin{aligned}
\ddot{x} &= 2\dot{y} + x - \frac{(1-\mu)(x+\mu)}{r_{13}^3} - \frac{\mu(x-1+\mu)}{r_{23}^3} - \frac{m_s(x-x_s)}{r_{s3}^3} - \frac{m_s}{a_s^3}x_s \\
\ddot{y} &= -2\dot{x} + y - \frac{(1-\mu)y}{r_{13}^3} - \frac{\mu y}{r_{23}^3} - \frac{m_s(y-y_s)}{r_{s3}^3} - \frac{m_s}{a_s^3}y_s \\
\ddot{z} &= -\frac{(1-\mu)z}{r_{13}^3} - \frac{\mu z}{r_{23}^3} - \frac{m_s(z-z_s)}{r_{s3}^3} - \frac{m_s}{a_s^3}z_s
\end{aligned} \tag{4}$$

where x, y and z are the components of $\bar{x}_{B_1}^{E-M\text{ Rotating}}$, $\dot{x}$, $\dot{y}$ and $\dot{z}$ are the components of $\dot{\bar{x}}_{B_1}^{E-M\text{Rotating}}$, the distance from P to Earth is labeled r_{13} and $r_{13} = \sqrt{(x+\mu)^2 + y^2 + z^2}$, the distance from P to the Moon is $r_{23} = \sqrt{(x-1+\mu)^2 + y^2 + z^2}$. The Sun's position vector with respect to the Earth-Moon barycenter B_1 is then,

$$\bar{r}_S = \begin{bmatrix} x_S \\ y_S \\ z_S \end{bmatrix}^T = \begin{bmatrix} a_s \left(\cos(\theta_s - \Omega)\cos(\Omega) \;\; -\sin(\theta_s - \Omega)\;\sin(\Omega)\;\cos(i) \right) \\ a_s \left(\cos(\theta_s - \Omega)\sin(\Omega) \;\; +\sin(\theta_s - \Omega)\;\cos(\Omega)\cos(i) \right) \\ a_s \;\sin(\theta_s - \Omega)\sin(i) \end{bmatrix}^T \tag{5}$$

where the superscript T indicates the transpose of a vector. Equations (4) and (5) describe the motion of the spacecraft P under the influence of the Earth, the Moon, and the Sun in the E-M rotating frame and expressed in nondimensional quantities.

The BCR4BP explicitly depends on time and therefore does not possess an integral of the motion. Thus, the 'energy' for P in the BCR4BP is not conserved. However, the instantaneous values of an energy-like quantity offer insights concerning the dynamical flow by exposing instantaneous forbidden regions and instantaneous equilibrium points. This energy quantity is defined in different frames: rotating Earth-Moon or rotating Sun-B_1 and with respect to the characteristic quantities. In the Earth-Moon rotating frame, the instantaneous energy E is evaluated as :

$$E = x^2 + y^2 + 2\frac{1-\mu}{r_{13}} + 2\frac{\mu}{r_{23}} + 2\frac{m_S}{r_{S3}} - 2\frac{m_S}{a_S^3}\left(x_S x + y_S y + z_S z\right) - (\dot{x}^2 + \dot{y}^2 + \dot{z}^2) \tag{6}$$

In the Sun-B_1 rotating frame, the energy H, or Hamiltonian, is:

$$\mathrm{H} = x'^2 + y'^2 + 2\frac{m_S - 1}{m_S\, r'_{S3}} + 2\frac{\mu}{m_s\, r'_{13}} + 2\frac{\mu}{m_S\, r'_{23}} - (\dot{x'}^2 + \dot{y'}^2 + \dot{z'}^2) \tag{7}$$

where x', y' and z' are the components of the position vector from the E-M-S system barycenter B_2, $\bar{x}_{B_2}^{S-B_1\text{ Rotating}}$, in the Sun-$B_1$ rotating frame; $\dot{x}'$, $\dot{y}'$ and $\dot{z}'$ are the components of the velocity vector in the same frame, and r'_{S3}, r'_{13} and r'_{23} are the norms of the primary-to-spacecraft vectors in the Sun-B_1 rotating frame. Note that E is computed using the state nondimensionalized with the E-M characteristic quantities, while H, the energy in the Sun-B_1 frame, is computed using the state nondimensionalized with respect to the CR3BP Sun-B_1 characteristic quantities (in the Sun-B_1 CR3BP, l^* is the distance between the Sun and the Earth-Moon barycenter, B_1, and m^* is the sum of the masses of the Sun, the Earth and the Moon).

Instantaneous equilibrium points exist in the BCR4BP. In the Earth-Moon vicinity, they correspond to the CR3BP E-M L_i equilibrium points perturbed by the Sun. Away from the Earth-Moon system, the CR3BP Sun-B_1 L_i are perturbed by the orbital motions of the Earth and the Moon. Using the CR3BP L_i as an initial guess and using a differential correction process, the BCR4BP instantaneous equilibrium points are straightforwardly located. At every instant, the locations shift due to the orientation of the Sun. Simultaneously, the value of the energy, i.e., H, is also changing which impacts an instantaneous set of zero velocity curves. Access to regions surrounding the Earth and the Moon through the Sun-B_1 L_1 and L_2 portals is summarized in Figure 4 for different solar orientations. Such information serves as a guide in assessing departure to heliocentric space.

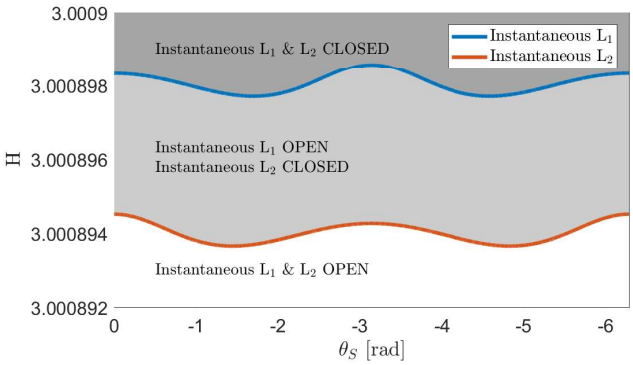

Figure 4: Instantaneous L_1 and L_2 energy in the BCR4BP.

The Ephemeris Model

For applications in mission scenarios where high-fidelity modeling accuracy is required, N-body differential equations and planetary ephemerides are employed. The N-body dynamics generally render the motion of a particle of interest (e.g., a spacecraft) in an inertial frame relative to a central body under the gravitational influence of the same central body and other additional perturbing bodies. Within this analysis, the relative position of each perturbing body with respect to the central body is instantaneously computed by employing NAIF SPICE ephemeris data. The Moon is selected as the central body for numerical integration in the J2000 inertial frame. The Earth and Sun are included as point masses, and the Moon's gravity is modeled using the GRAIL (GRGM660PRIM) model truncated to degree and order 8. Solar radiation pressure (SRP) is also included in the force model.

Operational errors on the spacecraft are considered in the higher-fidelity modeling. For multi-revolution propagations prior to a disposal maneuver, orbit maintenance maneuvers (OM maneuvers) are implemented. Each OM maneuver is associated with a navigation error on the spacecraft state: both low navigation errors of 1 km in position and 1 cm/s in velocity and larger navigation errors of 10 km in position and 10 cm/s in velocity are considered. Maneuver execution errors comprising 1.5% in magnitude, 1° in direction, and a fixed component of 1.42 mm/s are applied to each OM maneuver. Mismodeling in SRP assumptions provide 15% error in area and 30% error in coefficient of reflectivity. Momentum wheel desaturations are assumed to occur once per revolution near apolune with a translational ΔV component of 3 cm/s. In addition, the disposal maneuver is either applied error-free (no navigation or execution error considered) or it is applied with a 1.5% execution error and lower or higher navigation errors, as specified in each case. All values are 3σ and are implemented as Gaussian errors with zero mean.

NRHO: DEPARTURE AND DISPOSAL IN THE BCR4BP

Baseline Trajectories

The halo family and its subset, the Near Rectinilear Halo Orbits (NRHOs), are three-dimensional periodic orbits in the Circular Restricted 3-Body Problem (CR3BP). The halo family bifurcates from the planar Lyapunov family in the vicinity of each coplanar libration point. For the CR3BP equilibrium points L_1 and L_2 in the Earth-Moon system, the halo family members originate in the $x-y$ plane due to a bifurcation from the Lyapunov family, and evolve out of plane as they approach the Moon. The NRHO subset of the L_1 and L_2 halo families are defined by their linear stability properties.[6]. The Earth-Moon L_2 halo family appears in Figure 5(a).

The NRHO of interest in the current investigation is selected in part due to advantages for eclipse avoidance. Avoiding long eclipses due to the Earth shadow is of particular interest for the Gateway. Eclipses due

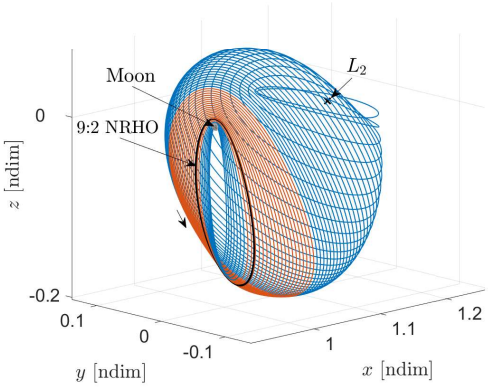

(a) **3D view of the CR3BP Earth-Moon L_2 halo family. The NRHO subset members are colored in orange. The 9:2 NRHO is plotted in black.**

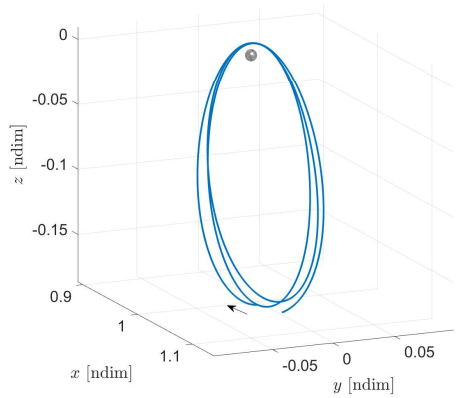

(b) **The 9:2 NRHO reconverged in the BCR4BP.**

Figure 5: **Baseline Trajectories in the E-M rotating frame**

to the Earth occur when the Sun, Earth, and spacecraft are aligned. This configuration occurs every synodic period of the Moon, which is approximately 29.4873 days. In this investigation, a 9:2 NRHO (9 revolutions in the orbit per 2 synodic periods of the Moon) is the baseline trajectory and, with appropriate phasing, eclipses due to Earth are avoided and lunar eclipses are rare. The 9:2 NRHO possesses a period of about 6.52 days and a perilune radius of 3157.8 km. Since the lunar radius is about 1737 km, the 9:2 NRHO, colored in black in Figure 5(a), is accessible.

In the BCR4BP, the NRHOs are not perfectly periodic, but the geometry can be maintained. Stacking multiple revolutions of selected CR3BP NRHOs and employing a corrections scheme to enforce continuity yields a continuous trajectory that maintains the geometry of the NRHO for some selected time interval. This stacking procedure is typically employed to transition a periodic orbit from the CR3BP to the ephemeris model[7]; it is also applicable when transitioning from the CR3BP to the BCR4BP. A non-homogeneous[8] stacking technique is applied to regulate the BCR4BP NRHO perilune radius. A differential corrections scheme is then used to reduce position and velocity discontinuities between consecutive arcs to an acceptable tolerance. The NRHOs reconverged in the BCR4BP preserve the original geometry and the altitude of the periapses, as observed in Figure 5(b).

Departure

The momentum integral[9] is a suitable metric to detect departure of the spacecraft from the NRHO. The momentum integral, MI, is evaluated as a line integral for the position vector between the initial time t_0, and the current time, t:

$$\mathrm{MI}_\Gamma(t) = \int_{t_0}^{t} x(\tau)\dot{x}(\tau) + y(\tau)\dot{y}(\tau) + z(\tau)\dot{z}(\tau)\, d\tau \tag{8}$$

where x, y, z are the position vector ($\bar{x}_{B_1}^{E-M\ \text{Rotating}}$) components in the Earth-Moon rotating frame, $\dot{x}$, $\dot{y}$, $\dot{z}$ are the velocity vector ($\dot{\bar{x}}_{B_1}^{S-B_1\ \text{Rotating}}$) components in the same frame, and τ is an independent time variable. The momentum integral over one period along a perfectly periodic orbit in the CR3BP is zero. In time-dependent models, such as the BRC4BP and the ephemeris model, the trajectory is not expected to precisely return to the initial state. Therefore, the momentum integral is not zero, but it remains bounded if the motion is bounded. To determine if the spacecraft has departed the NRHO, the momentum integral of the perturbed trajectory $\tilde{\Gamma}$ is evaluated and compared to the momentum integral for the reference trajectory Γ. In the current analysis, the reference trajectory Γ is selected as the NRHO without stationkeeping, and the perturbed trajectory $\tilde{\Gamma}$ is defined as the spacecraft trajectory with a disposal maneuver applied. The instantaneous difference between

their momentum integrals is defined as follows,

$$\Delta \text{MI}(t) = |\text{MI}_{\Gamma}(t) - \text{MI}_{\tilde{\Gamma}}(t)| \tag{9}$$

The perturbed trajectory remains in the vicinity of the reference trajectory for small ΔMI. Each application of the momentum integral employs a unique value for the metric that signals departure. For this investigation, the spacecraft is considered departed from the NRHO when the value of ΔMI exceeds 10^{-1}.

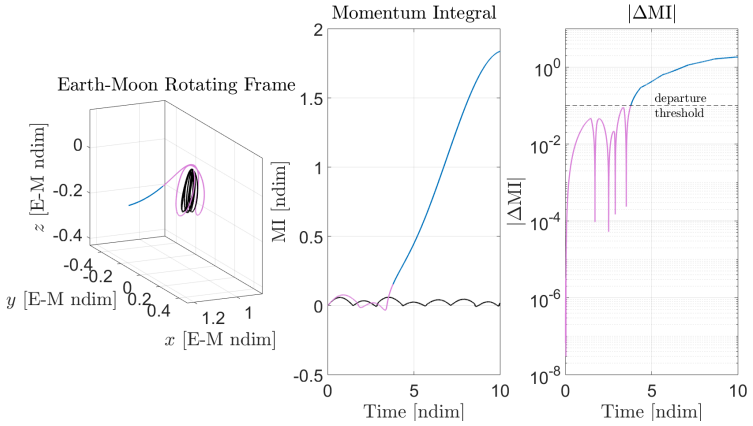

Figure 6: **Application of the Momentum Integral to define departure in the BCR4BP. The baseline trajectory is plotted in black. The actual trajectory, ΔV of 12 m/s implemented at perilune, is colored in pink when it remains in the vicinity of the NRHO, and in blue after departure from the NRHO. Note that the baseline also departs the NRHO at a later date since no stationkeeping is implemented.**

Disposal Framework

Definitions

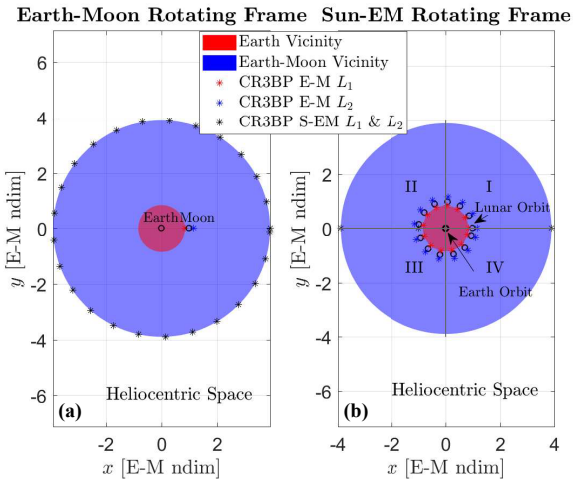

Figure 7: **The Earth-Moon vicinity, the Earth vicinity, and heliocentric space in the Earth-Moon rotating frame (a) and the Sun-B_1 rotating frame (b).**

The goal of the current disposal analysis is escape of the spacecraft from the Earth-Moon vicinity such that the vehicle enters and remains in heliocentric space. The Earth-Moon vicinity is defined as the region inside the CR3BP Sun-B_1 Hill region, that is, the sphere centered at the Earth-Moon barycenter (B_1) of radius approximately equal to the L_1 distance defined in the Sun-B_1 CR3BP. The Earth vicinity is the region within the sphere centered at the Earth with a radius approximate equal to the L_1 distance as defined in the Earth-Moon CR3BP. The Earth-Moon vicinity and the Earth vicinity appear in the Earth-Moon rotating frame and in the Sun-B_1 rotating frame in Figure 7. An escape, also denoted a 'success', is a trajectory that meets the following conditions after propagation for 365 days:

- Remains beyond the Earth vicinity.
- Crosses the boundary identifying the Earth-Moon vicinity only once (to exit and not return).

A capture (also labeled a 'failure' in this investigation) occurs when a trajectory does not satisfy at least one

of these conditions. Heliocentric space is the region exterior to the Earth-Moon vicinity and interior to the Sun orbit in the E-M rotating frame.

Quadrants

In the Sun-B_1 rotating frame, the direction of the net perturbing acceleration due to the Sun, denoted the tidal acceleration, on a spacecraft in an orbit about the B_1, i.e., the Earth-Moon barycenter, depends on the orientation of the orbit relative to the Sun and the Earth-Moon system. A set of quadrants, centered at B_1, is defined to facilitate the investigation of the tidal acceleration.[10]. The quadrants are defined in the Sun-B_1 rotating frame, as illustrated in Figure 8. When the spacecraft orbit is viewed in the Sun-B_1 rotating frame, its orientation is defined by the quadrant that includes the apoapsis along a given revolution. The effects of the tidal acceleration are greatest near apoapsis. Assuming a prograde orbit:

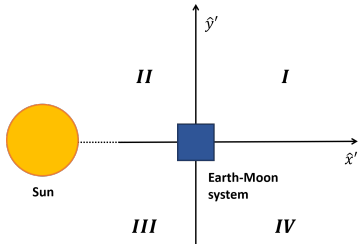

Figure 8: Quadrants as defined in the Sun-B_1 rotating frame.

- In quadrants I and III, the perturbations generally oppose the direction of the motion. As a result, solar effects tend to elongate the orbit and decrease the periapse radius.
- In quadrants II and IV, the tidal perturbations are generally along the direction of the motion. The orbit tends to circularize and the periapse tends to increase.

The location of a trajectory's apoapses within the quadrants influence the Sun's tidal effects. However, note that the Sun's perturbing effect is the largest on a spacecraft moving in the Sun-B_1 plane, while the disposal trajectory may possess non-zero z' components. In this investigation, trajectories are propagated for a year after the disposal maneuver time. Escape trajectories may, in fact, return to the Earth-Moon vicinity after the one-year propagation; this possibility is not investigated in the current analysis document.

RESULTS IN THE BCR4BP

Multiple factors influence the disposal trajectory and its assessment as a success (escape) or a failure (capture). These effects include: the location of a trajectory apoapsis within the quadrants, the energy of the trajectory, and the orbit's osculating eccentricity with respect to B_1. The osculating eccentricity is defined as the instantaneous eccentricity of the trajectory with respect to B_1 in the Sun-B_1 frame; since the spacecraft orbit is not Keplerian relative to B_1, the eccentricity is varying. To escape the Earth-Moon vicinity, the Sun-B_1 portals near L_1 and L_2 must be open, so the energy level H of the trajectory must be below the value corresponding to L_1 (if escaping through L_1) or L_2 (if escaping through L_1 or L_2). The same reasoning applies for the osculating eccentricity with respect to B_1: if the eccentricity is less than 1, i.e., the trajectory is captured around B_1; if the eccentricity drifts above 1, the trajectory is hyperbolic with respect to B_1 in the Keplerian sense. Factors that do not significantly influence the escape include the altitude of the NRHO perilune or the magnitude of the ΔV maneuver. While increasing the ΔV magnitude tends to decrease the time to depart the NRHO, it does not guarantee an escape: escapes exist for $\Delta V = 1$ m/s and captures occur at $\Delta V = 100$ m/s. These elements reaffirm that the disposal problem is a Sun-B_1 problem.

The analysis for the disposal is framed in terms of the trajectory evolution. The disposal ΔV maneuver is implemented at perilune on the NRHO in the rotating velocity direction. Depending on the magnitude of the ΔV, the spacecraft may or may not complete post-maneuver revolutions along the NRHO. Once departed from the NRHO, the spacecraft is in the Earth-Moon vicinity. Depending on the previously identified factors, the fate of the trajectory is labeled as one of the following:

- **Direct Escape:** Directly catch the departing flow.
- **Indirect Escape:** Additional E-M apopases but eventually catch the departing flow.
- **Capture:** Additional E-M apopases but do not catch the departing flow, or impact the Moon/the Earth.

Each outcome is detailed in the next subsections.

Direct Escape

Direct escape trajectories directly leave the Earth-Moon vicinity after departing the NRHO. These direct escapes emerge as a consequence of attaining the correct energy level once departed from the NRHO, that is, the Sun-B_1 gateways are open. An example of direct escape appears in Figures 9 and 10. In this example, a maneuver of magnitude $\Delta V = 1$ m/s is implemented at perilune in the rotating E-M velocity direction. The spacecraft evolves along 4 additional revolutions in the NRHO before departing (in all the following figures, lines colored in pink indicates the spacecraft remains on the NRHO, because $\Delta\text{MI}(t) < 10^{-1}$). Four apoapses with respect to B_1, marked by red dots and numbered in Figures 9 and 10, occur during the post-maneuver revolutions. Once the spacecraft departs the NRHO, it is moving in Earth-Moon space. In all

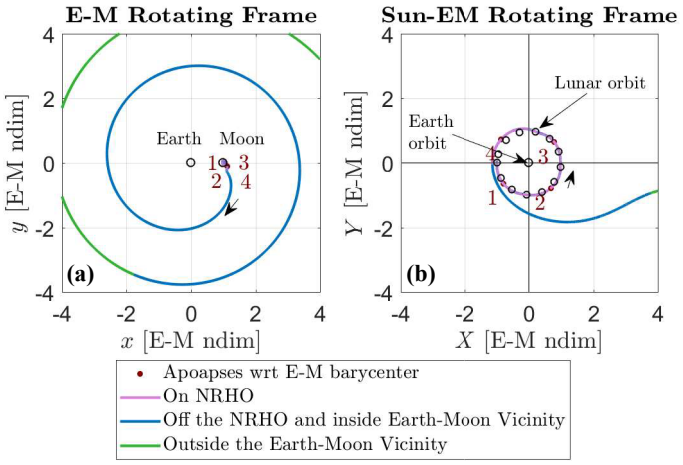

Figure 9: **A direct escape for $\Delta\mathbf{V} = 1$ m/s in the BCR4BP, as seen in the E-M rotating frame (a) and the Sun-B_1 rotating frame (b).**

the following figures, the lines corresponding to the spacecraft motion off the NRHO but still inside the Earth-Moon vicinity are colored in blue. The lines corresponding to the spacecraft path that is off the NRHO and beyond the Earth-Moon vicinity (in heliocentric space) are colored in green. In Figure 9(a), the trajectory escapes the Earth-Moon vicinity through the instantaneous Sun-B_1 L_2 portal. The energy history along the trajectory, plotted in Figure10, indicates that L_1 and L_2 are open when the spacecraft departs the NRHO. Note that the energy is constant after the spacecraft escapes the Earth-Moon vicinity. In heliocentric space, the influence of the Earth and Moon circular motion on the spacecraft trajectory is minimal; the BCR4BP energy is approximated by the CR3BP Sun-B_1 Jacobi Constant.

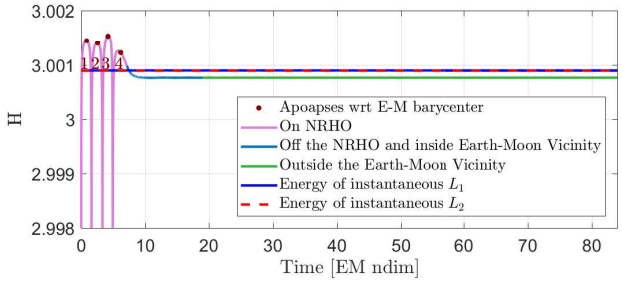

Figure 10: **Energy history of the direct escape trajectory in the Sun-B_1 frame.**

Indirect Escape

Indirect escapes possess at least one additional apoapse with respect to the Earth-Moon barycenter, B_1, before escaping the Earth-Moon vicinity. The tidal effects from the Sun change the energy and the eccentricity

of the trajectory, which then enables to escape. An example of indirect escape appears in Figures 11 and 12. A disposal maneuver of magnitude $\Delta V = 7$ m/s is implemented at the first perilune. Because the maneuver magnitude is higher than in the previous example (Figure 9), the spacecraft completes only two

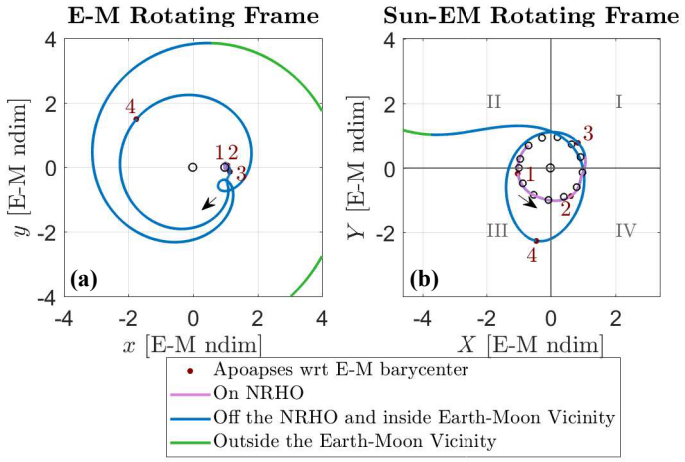

Figure 11: **An indirect escape for $\Delta \mathbf{V} = 7$ m/s in the BCR4BP, as seen in the E-M rotating frame (a) and the Sun-$\mathbf{B_1}$ rotating frame (b).**

post-maneuver revolutions along the NRHO before departure. The first two apoapses, labeled 1 and 2, occur while the spacecraft is still on the NRHO, therefore, they are not included in the tidal effect analysis. At the third apoapse, the spacecraft has departed from the NRHO. This apoapse and the following, 4, are located in quadrant I and quadrant III, respectively. Recall that in these two quadrants, perturbations generally oppose the direction of the motion in a prograde orbit. The osculating eccentricity increases after apoapses 3 and 4, as apparent in Figure 12(b). After periapse 4, the osculating eccentricity surpasses one, the trajectory is now hyperbolic with respect to the Earth-Moon barycenter, B_1 and the spacecraft escapes the Earth-Moon vicinity. The energy of the trajectory in the Sun-B_1 frame, in Figure 12(a), is also insightful. After departure from the NRHO, the energy is too low (equivalently, H is too high) and both the instantaneous L_1 and L_2 portals are closed. The energy increases after apoapse 3 and apoapse 4; after the last apoapse, the energy is higher than the energy of the instantaneous L_1 and L_2 and the spacecraft escapes.

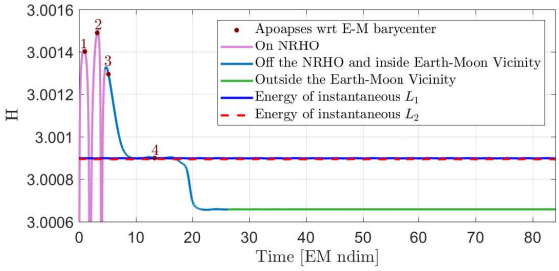

(a) **Energy history of the indirect escape trajectory in the Sun-$\mathbf{B_1}$ frame.**

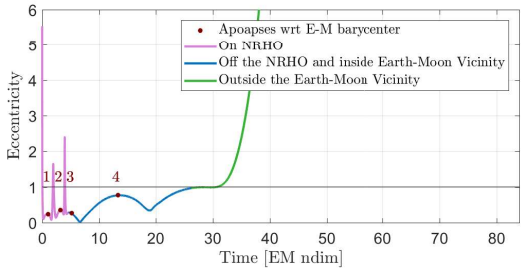

(b) **Osculating eccentricity with respect to $\mathbf{B_1}$ of the indirect escape trajectory in the Sun-$\mathbf{B_1}$ frame. The black line indicates the eccentricity equal to 1.**

Figure 12: **Indirect escape trajectory energy and osculating eccentricity in the Sun-$\mathbf{B_1}$ rotating frame.**

Capture

Capture trajectories do not escape in the one-year timespan or they enter the vicinity of the Earth, the sphere centered at B_1 of radius approximately equal to the Earth-Moon CR3BP L_1 distance. The captures possess an energy level when they depart the NRHO such that the instantaneous L_1 and/or L_2 are closed.

An example of capture is demonstrated in Figures 13 and 14. Lunar flybys modify the trajectory dynamics and can potentially offset the tidal effect gained at the apoapses. After apoapse 3, the spacecraft re-enters the Earth-Moon vicinity, as noted in Figure 13; the trajectory is, therefore, categorized as a capture. The trajectory is propagated after apoapse 3 to investigate whether an escape occurs. Though the tidal effects and flybys of the primary influence on the spacecraft, the trajectory never achieves the correct combination of eccentricity, energy, and orientation to escape. Additionally, the spacecraft falls into a resonant structure with close passes to the Earth, as in Figure 13(a). The flybys of the Earth are characterized by the peaks in energy H in Figure 14(a) between apoapses 6 and 7, apoapses 9 and 10, and after apoapse 10. In this example, the spacecraft does escape the Earth-Moon vicinity beyond a 2 year interval with multiple lunar and Earth flybys; nevertheless, this trajectory does not qualify as a safe disposal option.

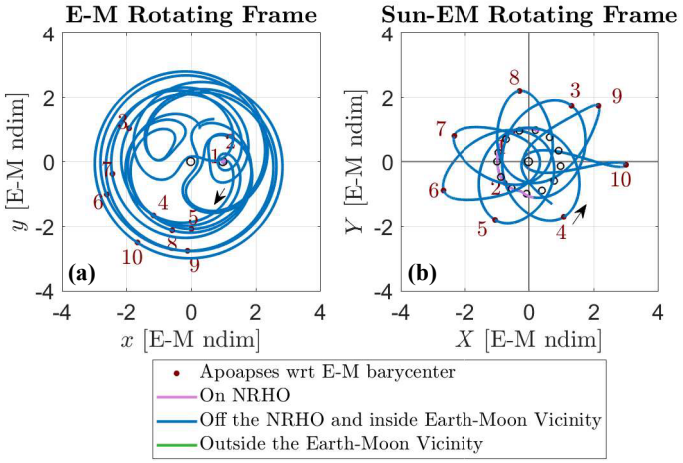

Figure 13: **A capture trajectory propagated for 1.25 years with a disposal maneuver $\Delta V = 7$ m/s in the BCR4BP, as seen in the E-M rotating frame (a) and the Sun-B_1 rotating frame (b).**

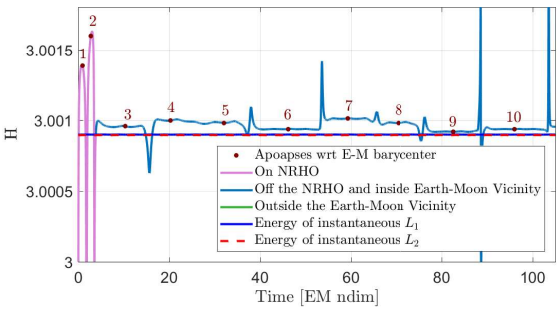

(a) **Energy history of the capture trajectory in the Sun-B_1 frame.**

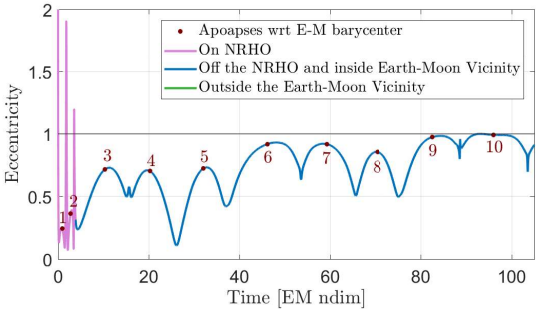

(b) **Osculating eccentricity with respect to B_1 of the capture trajectory in the Sun-B_1 frame. The black line indicates the eccentricity equal to 1.**

Figure 14: **Indirect escape trajectory energy and osculating eccentricity in the Sun-B_1 rotating frame.**

NRHO: DEPARTURE AND DISPOSAL IN THE EPHEMERIS MODEL

Predictions from the BCR4BP effectively describe trajectory behavior and trends in the ephemeris force model. These predictions are applied to Gateway mission scenarios in the higher-fidelity ephemeris model to generate specific examples of successful LM disposal scenarios. First, the problem is framed in terms of the reference NRHOs employed in the analysis. The post-maneuver time to NRHO departure is explored, and then sample scenarios representing direct escape, indirect escape, and capture are generated. Finally, a detailed exploration of LM disposal focuses on a 1 m/s disposal maneuver and a 15 m/s disposal maneuver.

Baseline Trajectories

Properties of disposal trajectories in the sensitive cislunar regime, in which the gravitational effects of the Sun, Earth, and Moon are simultaneously significant, depend on the quality of the reference NRHO trajectory. Employing a well-converged reference trajectory in the analysis is important to ensure the spacecraft is not already on a path departing from the NRHO before the disposal maneuver is applied. For the current analysis, long-horizon reference NRHOs are generated in the ephemeris model through a forward-backward shooting process that takes patch points from the CR3BP NRHO and converges them into the ephemeris force model[11]. As in the BCR4BP, the perfectly periodic CR3BP NRHO becomes a quasi-periodic NRHO in the ephemeris model, but it retains properties of the original periodic orbit. The primary reference orbit is a 9:2 lunar synodic resonant NRHO phased to avoid eclipses by the Earth. The reference trajectory extends for 15 years with an initial epoch in January 2020. Additional reference orbits are also examined to confirm that results are not specific to an individual reference NRHO; each extends for over a year in an approximate 9:2 resonance with the lunar synodic period. Starting epochs range from January 2020 to May 2023. Prior to a disposal maneuver, the reference spacecraft is maintained in the NRHO via an x-axis crossing control orbit maintenance (OM) algorithm[7,9,12] with small burns at apolune. After the disposal, the spacecraft is ballistically propagated until departure from the NRHO is achieved and escape/capture outcomes are determined.

Departure

As demonstrated in the BCR4BP analysis, the location of the Sun after the spacecraft departs from the NRHO determines, in part, the long-term destination of the spacecraft. Thus, the epoch of departure from the NRHO is critical to the spacecraft's fate. Additionally, the more post-burn revolutions the spacecraft experiences in or near the NRHO, the more opportunity there is for small variations in the orbit to change the actual epoch of departure. Understanding the duration of time spent in the vicinity of the NRHO after a disposal maneuver is thus a key to designing disposal scenarios with the desired outcome. Multiple factors affect the time to depart the NRHO; factors include quality of the converged reference NRHO, maneuver location along the NRHO, and magnitude and direction of the disposal maneuver. The definition of departure from the NRHO influences the assessment of the time for a perturbed orbit to depart. In the current investigation, a trajectory is considered to have departed the NRHO when it is no longer following the quasi-periodic path around the Moon but is still in the Moon's vicinity. After departing the NRHO, a trajectory may remain bounded in the vicinity of the Earth, it may escape to heliocentric space, or it may impact one of the primaries. As in the BCR4BP, NRHO departure is defined according to the divergence of the momentum integral, but the selection of a the specific threshold can vary depending on the characteristics of particular departing trajectory.

The first parameter explored is the quality or stability of the converged reference orbit in the ephemeris force model. The 'quality' is defined as the time interval for an uncontrolled spacecraft to remain in the NRHO before departure, as defined by divergence of the momentum integral. To quantify the time to departure, the spacecraft is maintained in the NRHO in the presence of navigation errors (10 km in position, 10 cm/s in velocity, 3σ), maneuver execution errors, wheel desaturation errors, and SRP errors as previously defined. After a given number of revolutions in the NRHO, the orbit maintenance is turned off and the spacecraft is propagated to departure. Fifty Monte Carlo trials are run for each of four cases, in which orbit maintenance

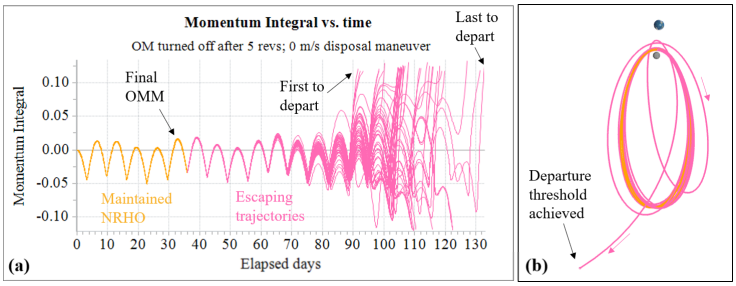

Figure 15: **Momentum Integral histories for 50 Monte Carlo trials with no disposal maneuver (a), sample escaping orbit (b).**

ceases after 2, 3, 4, or 5 revolutions in the NRHO. The time histories of the MI for the 50 Monte Carlo trials in the final case appear in Figure 15. After 5 revolutions in the NRHO, represented in orange, the final orbit maintenance maneuver (OM maneuver) is implemented at apolune and each trajectory is propagated forward uncontrolled, as plotted in pink. After about 6 more revolutions near the NRHO, the 50 trials start to diverge from one another. The first trial to depart the vicinity of the NRHO does so 70 days after OM is ceased, or after 8 additional revolutions near the NRHO. The final trial to depart remains in the vicinity of the NRHO for 114.3 days, over 6 revolutions longer. The minimum, mean, and maximum times to depart in the four cases appear in Table 1. The mean times to escape are relatively consistent, ranging from 72.4 days to 76.2 days in the NRHO vicinity. However, the mean and maximum times to escape vary widely. Additionally, time to depart a poorly-converged NRHO is significantly faster. Without a disposal maneuver, the epoch of departure from the vicinity of the NRHO (and hence the final destination of the departing spacecraft) is unpredictable based on the time of OM cessation. A sample trajectory that escapes after 84 days appears in Figure 15(b) with the point of departure marked for reference.

Table 1: **Days to NRHO departure. OM maneuvers for 2-5 revolutions, no error applied to disposal burns.**

Days to NRHO Departure: no error applied to disposal burns. 50 trials per case.															
	0 m/s disposal			1 m/s disposal			5 m/s disposal			10 m/s disposal			15 m/s disposal		
rev	min	mean	max	min	mean	max	min	mean	max	min	mean	max	min	mean	max
2	55.6	74.7	114.2	39.4	40.0	40.4	17.3	17.4	17.5	22.1	22.5	23.3	13.5	13.6	13.8
3	59.3	76.2	107.7	36.7	37.8	39.0	16.9	17.0	17.0	12.8	13.0	13.0	13.0	13.1	13.1
4	56.7	72.4	102.9	38.3	38.8	39.0	18.1	18.3	18.4	11.9	11.9	12.1	12.3	12.3	12.4
5	70.0	74.5	114.3	38.2	38.8	39.3	17.6	17.8	17.9	13.4	13.5	13.7	12.9	13.0	13.0

Table 2: **Days to NRHO departure. OM maneuvers for 2-5 revolutions, navigation/execution error applied to disposal burns.**

Days to NRHO Departure: navigation and maneuver execution errors applied to disposal burns. 50 trials per case															
	0 m/s disposal			1 m/s disposal			5 m/s disposal			10 m/s disposal			15 m/s disposal		
rev	min	mean	max	min	mean	max	min	mean	max	min	mean	max	min	mean	max
2	55.6	74.7	114.2	30.5	40.4	60.0	17.6	18.0	19.1	14.4	25.7	53.8	13.8	14.1	14.2
3	59.3	76.2	107.7	30.6	37.5	63.3	17.3	17.5	17.7	13.0	13.8	39.9	13.2	13.4	13.7
4	56.7	72.4	102.9	30.0	37.7	66.6	18.8	19.9	27.3	12.1	12.2	12.7	12.5	12.7	12.9
5	70.0	74.5	114.3	29.4	37.4	64.4	18.1	18.4	19.4	13.3	14.3	31.4	13.1	13.3	13.5

The time to depart the NRHO is significantly more consistent when an accurate disposal maneuver is applied, however, the maneuver location along the NRHO has a substantial impact on departure time. In general, an NRHO is most sensitive to perturbations near perilune. Thus, for a spacecraft in long-term operations in an NRHO, perturbations near the Moon are to be avoided. However, for a spacecraft departing the NRHO, a disposal maneuver near perilune is the most effective for fast departure from the orbit. To characterize the dependency of departure time on maneuver location, a set of departure cases is run for maneuvers at various values of true anomaly (TA) around multiple revolutions the NRHO. In each case, a 1 m/s burn in the velocity direction is applied to the spacecraft without including navigation or execution errors, which is then propagated to NRHO departure. Stepping along the NRHO in 5° increments, the process is accomplished for nine revolutions of the NRHO. The results appear in Figure 16(a). The maximum escape times consistently occur just prior to apolune. Surrounding apolune, at values of TA between approximately 100° and 240°, times to depart the NRHO vary considerably from one TA to the next; that is, a small change in maneuver TA leads to a large difference in departure time. Spikes in the trends are visible around 120° and 210°; these spikes correspond to trajectories that include several large additional revolutions around the Moon prior to departing. In contrast, near perilune, departure times are consistently about 30-32 days. For maneuvers near perilune, small variations in maneuver TA do not significantly alter the time to depart. For predictable departure times, maneuvers near perilune are the most consistent. The patterns in departure time as a function of TA continue as the maneuver ΔV is increased. In Figure 16(b), the time between the disposal burn and departure from the NRHO appear as a function of TA for maneuver magnitudes ranging from 1 m/s

to 10 m/s. Each burn is implemented after two revolutions of OM maneuvers in the NRHO. Always, the longest time to escape is just before apolune, and a flat slope in departure time surrounds perilune.

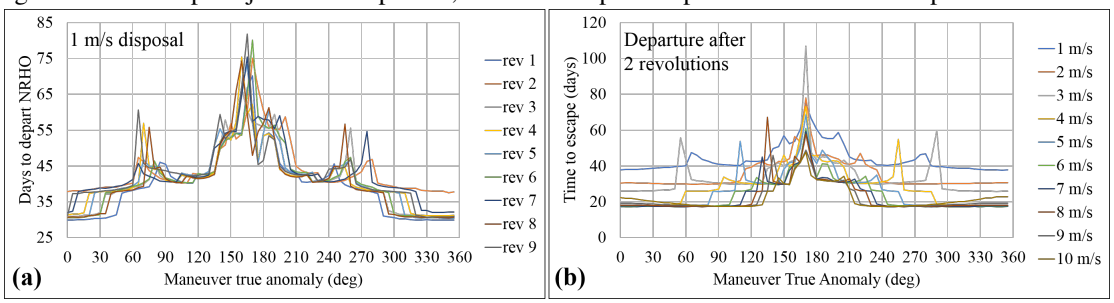

Figure 16: **Days to depart the NRHO as a function of maneuver TA around nine revolutions of the NRHO after a 1 m/s disposal burn (a). Days to depart the NRHO as a function of maneuver TA after 2 revolutions for varying maneuver magnitudes (b).**

From this point onward, the disposal maneuver is assumed to occur at perilune, and trends in departure time as a function of maneuver magnitude are investigated. In general, as the size of the disposal burn increases, the time to depart decreases, but the pattern is not linear. For maneuver magnitudes ranging from 1 m/s to 20m/s, Monte Carlo analyses are run for departure burns after 2, 3, 4, and 5 revolutions in the NRHO. Fifty trials are run per case with navigation (10 km in position, 10 cm/s in velocity, 3σ) and spacecraft errors applied during orbit maintenance as previously described. Two scenarios are considered: the first assumes a perfect disposal maneuver unperturbed by navigation or execution errors; the second applies a 10 km, 10 cm/s (3σ) navigation error and a 1.5% maneuver execution error at the disposal burn. Minimum, mean, and maximum times to departure from the NRHO for each case appear in Figure 17. With a perfect disposal maneuver, as in Figure 17(a), results are relatively consistent, though some variations are apparent caused by spacecraft and navigation errors applied prior to the maneuver. The times to depart without a maneuver, as previously noted, are large and vary considerably between trials. The time to depart quickly falls and becomes more consistent as a maneuver is added. As the maneuver size increases, the time to depart tends to decrease as a step function, with the escape occurring after a discrete number of revolutions near the NRHO. Depending on the specific perilune within the reference NRHO that contains the disposal maneuver, the step down to a lower departure time occurs at different maneuver magnitudes. The minimum, mean, and maximum times to escape for error-free 1 m/s, 5 m/s, 10 m/s and 15 m/s disposal burns appear in Table 1. The second scenario, pictured in Figure 17(b), assumes navigation and maneuver execution errors affect the disposal burn. In this case, the time to depart is significantly less consistent for disposal maneuvers smaller than 12 m/s. Minimum, mean, and maximum times to escape for 1 m/s, 5 m/s, 10 m/s, and 15 m/s disposal burns appear in Table 2 with maneuver execution errors and navigation errors of 10 km and 10 cm/s (3σ) applied to the disposal burn. Note significantly larger variations in the times to departure, especially for maneuver magnitudes of 1 m/s and 10 m/s. The uncertainty in departure time is mitigated by decreasing the navigation errors associated with the burn or increasing the size of the disposal burn. Further discussion appears below.

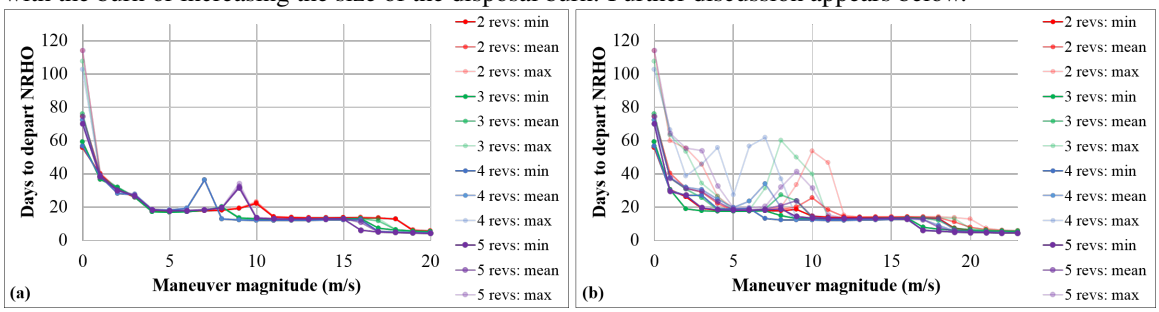

Figure 17: **Error-free disposal burn (a) and disposal burn with errors considered (b).**

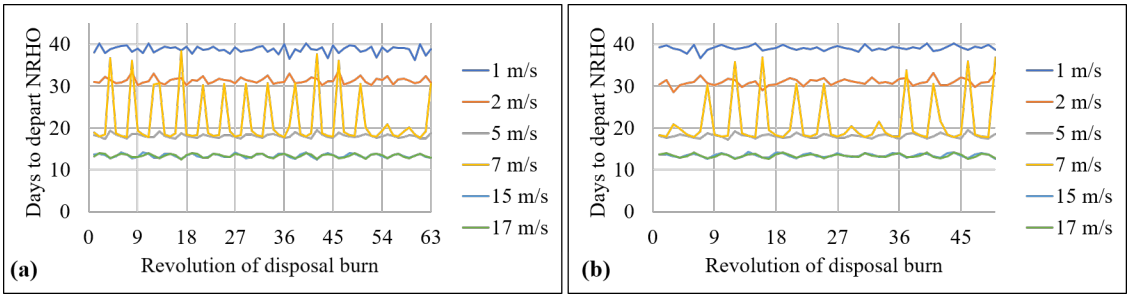

Figure 18: **Time to NRHO departure measured from the disposal burn for several ΔV magnitudes. Disposal burn occurs after 1 to 63 revolutions within the NRHO. Baseline reference NRHO (a) and secondary reference NRHO (b).**

Finally, to complete the exploration of the NRHO departure behavior, single Monte Carlo trials are run for various maneuver magnitude values applied consecutively over 63 revolutions of the NRHO. That is, a 1 m/s disposal burn is applied after the first revolution in the NRHO and propagated to departure. The process is repeated by applying a disposal burn after two maintained revolutions in the NRHO and propagating to departure, then after three revolutions, four, and so on until in the final case, the spacecraft spends 63 revolutions, or 447 days, orbiting in a maintained NRHO prior to the departure maneuver. In each case, the time to depart is recorded and consistency is examined across the disposal maneuver epochs. Departure times for six selected values of disposal burn magnitude appear in Figure 18. For five of the six burn magnitudes, the time from disposal burn to NRHO departure is consistent across the 63 revolutions. For a 7 m/s disposal burn, however, the departure time has variations between disposal burn revolutions. Figure 18(a) corresponds to the baseline 15-year 9:2 lunar synodic resonant NRHO, with an initial epoch in January 2020. The process is repeated for a second reference trajectory to assess the dependence of results on a particular reference NRHO. The second reference is also in a 9:2 resonance with the lunar synodic period, but it is not phased to avoid eclipses, and it has an initial epoch in May 2023. The patterns in the time to depart the NRHO are consistent across all the burn magnitudes investigated.

RESULTS IN THE EPHEMERIS MODEL

For LM disposal from the Gateway, direct escapes to heliocentric space are of interest to avoid interfering with assets either at the Moon or Earth. As in the BCR4BP, the spacecraft's energy, location within the quadrants, and osculating eccentricity affect the outcome of the disposal. The time to depart the NRHO combined with the epoch of the departure burn determine the location of the departing trajectory within the quadrants in the Sun-B_1 frame. Samples of direct escapes to heliocentric space, indirect escapes, and captured trajectories that remain earthbound illustrate the applicability of the BCR4BP analysis in the higher-fidelity ephemeris model.

Direct Escape

Disposal trajectories that directly escape into heliocentric space are candidate end-of-mission paths for LMs. One example appears in Figure 19. After two revolutions of orbit maintenance in the NRHO, a disposal maneuver of 1 m/s in the velocity direction is executed at perilune. Ten sample Monte Carlo trials appear in the Sun-B_1 rotating frame in Figure 19(a) and in the Earth-Moon rotating frame in Figures 19(b) and 19(d). Spacecraft errors and navigation errors (10 km in position, 10 cm/s in velocity) are considered during orbit maintenance, and an error-free disposal maneuver is applied. The orange curve represents the maintained revolutions in the NRHO. The pink portions of the trajectories correspond to post-maneuver revolutions in the Earth-Moon vicinity, and blue lines occur outside the Moon's vicinity but still in the Earth-Moon region. The color changes to green when the trajectories escape the Hill region associated with the Earth. In Figure 19(b), the revolutions in the maintained NRHO and the post-maneuver revolutions near the Moon are apparent looking down the x-axis towards the Earth in the Earth-Moon rotating frame. In Figure 19(d), a wide, top-down view of the Earth-Moon rotating frame illustrates

the escape from the Earth-Moon vicinity. The trajectories diverge slightly over time due to small differences in their post-disposal maneuver states, but they all exit the vicinity of the Earth to heliocentric space. Each trajectory passes through its final perigee in quadrant III in the Sun-B_1 rotating frame (marked by a black arrow in Figure 19(a)), elongating the orbit as it escapes the Earth's vicinity through the Sun-B_1 L_2 portal. In Figure 19(c), the Sun-B_1 energy appears as a function of time. The energy values associated with the L_1 and L_2 libration points in the Sun-B_1 system appear as a black line, indistinguishable at this scale. As the spacecraft departs the NRHO, its energy lies below that associated with the Sun-B_1 L_1 point (Figure 19(b)), providing for an open portal at L_2 that allows escape from the Earth-Moon region. Because the propagations occur in the ephemeris force model, the value of energy is not constant, as it would be in the Sun-B_1 CR3BP. The large perturbations to the energy value by the Moon are apparent as spikes in the orange and pink revolutions near the Moon for the first 50 days. The energy trend flattens as the spacecraft departs the vicinity of the Moon, but it grows slightly over time due to the eccentricity of the Earth's orbit, eventually closing off the portal at L_2.

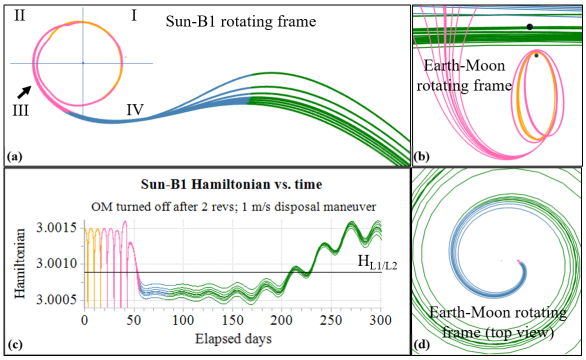

Figure 19: Direct escapes in the Sun-B_1 rotating frame with a 1 m/s burn after 2 revolutions in the NRHO (a), Evolution of the Sun-B_1 energy over time (c), direct escapes in the Earth-Moon rotating frame (b), (d).

Indirect Escape

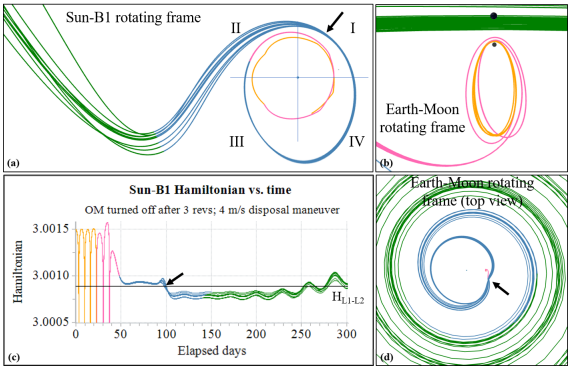

Figure 20: Indirect escapes in the Sun-B_1 rotating frame with a 4 m/s burn after 3 revolutions in the NRHO (a), Evolution of the Sun-B_1 energy over time (c), indirect escapes in the Earth-Moon rotating frame (b), (d).

As in the BCR4BP, the complex dynamics affecting the post-departure regime in the ephemeris model lead to certain trajectories escaping, not immediately, but after several revolutions around the Earth. One such example appears in Figure 20. In this example, a 4 m/s disposal maneuver is applied in the velocity direction at perilune after three maintained revolutions in the NHRO. Ten sample Monte Carlo trials, assuming navigation and spacecraft errors during orbit maintenance and an error-free disposal maneuver, are propagated forward, and none escapes immediately from the vicinity of the Earth. The maintained orbits in the NRHO appear in orange, with post-maneuver revolutions in the vicinity of the Moon appearing in pink. After departing the NRHO, the first apogee occurs near the quadrant III-quadrant IV border, seen in Figure 20(a), at which point the energy is higher than the value associated with L_1. The energy drops below the threshold after about 100 days, when the trajectory is near perigee in quadrant I. At this point, marked by a black arrow in Figures 20(a), 20(c), and 20(d), the trajectory makes a close approach to the Moon, as apparent in the Earth-Moon rotating view in Figure 20(d). The Moon perturbs the energy, dropping its value below the L_1 threshold and opening a portal to escape, as apparent in the time history of the energy in Figure 20(c). After this point, the trajectory catches the flow escaping to heliocentric space, exiting the Earth-Moon vicinity

when the trajectories transition from blue to green in the Sun-B_1 rotating view in Figure 20(a).

Capture

When the post-departure orientation is not appropriately aligned or the trajectory is insufficiently energetic, the trajectory remains bounded in the Earth-Moon system. A sample case appears in Figure 21. Ten sample Monte Carlo trials are performed by applying an error-free 2 m/s disposal burn after 2 maintained revolutions in the NRHO. While each trajectory passes through apses in quadrants I and III, as apparent in Figure 21(a), the energy is never sufficiently low to allow escape at either L_1 or L_2. That is, the energy in Figure 21(c) remains always above the black line representing the energy value corresponding to the L_1 libration point in the Sun-B_1 system. In contrast to the indirect escape, with a close approach to the Moon to reduce the Hamiltonian, the capture trajectory does not pass sufficiently close to the Moon after departing the NRHO, as is apparent in 21(d). The views in the Earth-Moon rotating frame in Figures 21(b) and 21(d) demonstrate that the trajectories remain bounded in the Earth-Moon vicinity.

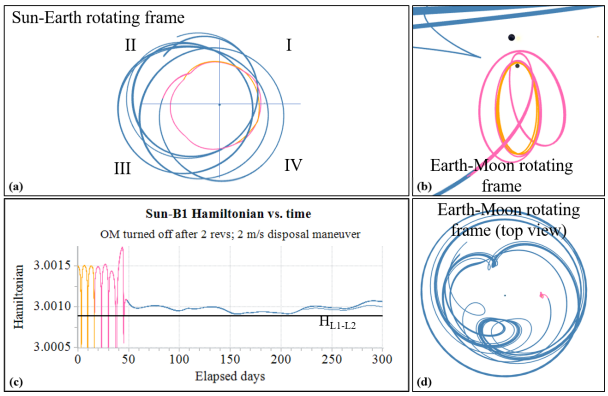

Figure 21: **Captured orbits in the Sun-B_1 rotating frame with a 2 m/s burn after 2 revolutions in the NRHO (a), Evolution of the Sun-B_1 energy over time (c), captures in the Earth-Moon rotating frame (b), (d).**

Impacts

In some cases, disposal maneuvers applied at perilune result in impact with the Moon or the Earth. Lunar impact can occur prior to departure from the vicinity of the Moon, or the LM can depart from the Moon's vicinity and then re-enter the lunar vicinity and impact. Two examples appear in the Earth-Moon rotating frame in Figure 22. The first example, in Figure 22(a), represents an impact after the disposal maneuver but before departure from the vicinity of the Moon. The impact orbit in Figure 22(a) occurs when a disposal maneuver of 15 m/s in the anti-velocity direction is applied at perilune after four maintained revolutions in the NRHO. After the disposal maneuver, the LM continues in orbit around the Moon for two more revolutions, after which it impacts the Moon at perilune. In the second lunar impact example, appearing in Figure 22(b), a 5 m/s disposal burn in the velocity direction is executed after six maintained revolutions in the NRHO. The spacecraft exits the lunar vicinity

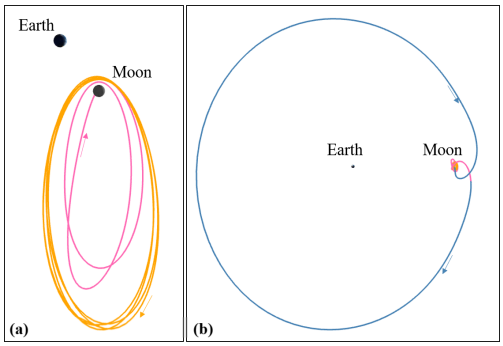

Figure 22: **Lunar impact trajectories in the Earth-Moon rotating frame. Direct impact after a 15 m/s maneuver in the anti-velocity direction (a), resonant orbit impact after a 5 m/s maneuver in the velocity direction (b).**

in a resonant orbit with the Moon's period around the Earth; two months later, it returns to the Moon on an impact trajectory.

Certain disposal trajectories that do not escape to heliocentric space are observed to impact the Earth. Two examples appear in the Sun-B_1 rotating frame in Figure 23. Both resemble ballistic lunar transfers (BLTs) in reverse. For a spacecraft departing from the Earth, BLTs employ solar gravity to raise perigee to the radius of the Moons orbit by placing apogee in quadrant II or IV. Whitley et al.[13] explore BLTs for Earth to NRHO transfers. In contrast, the two examples in Figure 23, starting from an NRHO and exiting the lunar vicinity with apogee in quadrants I and III, are affected by solar gravity such that the perigee is lowered to impact Earth. In Figure 23(a), a maneuver of 17 m/s is applied in the velocity direction at perilune after two revolutions in the NRHO. An apogee in quadrant I leads to Earth impact at the subsequent perigee. Similarly, in Figure 23(b), a maneuver of 10 m/s in the velocity direction is executed after two revolutions in the NRHO. After passing through apogee in quadrant III, the LM impacts Earth at its subsequent perigee. While unexpected impacts are to be avoided, these impact examples demonstrate that trajectories that intersect with both the Earth and Moon are available with low ΔV departure maneuvers. Such trajectories may be desirable for certain applications.

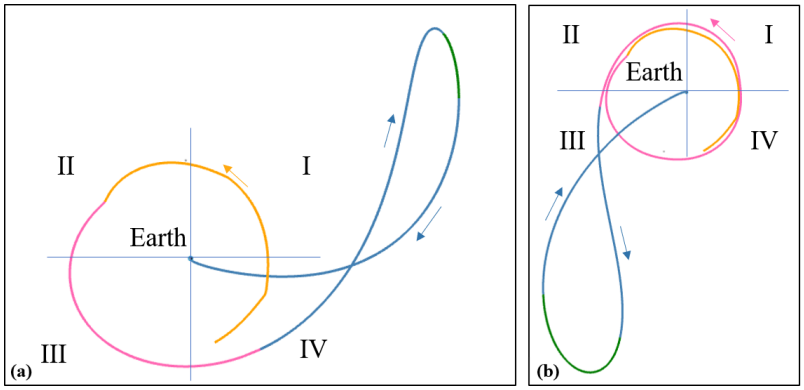

Figure 23: **Impacts with Earth in reverse ballistic lunar transfers in the Sun-B_1 rotating frame after a 17 m/s disposal maneuver (a) and a 10 m/s disposal maneuver (b).**

Maneuver Phasing and Heliocentric Escapes

As demonstrated, the time between the disposal maneuver and the departure from the NRHO depends on the reference NRHO, the maneuver magnitude, direction, and location, and errors present in the flown trajectory, among other parameters. Then, orienting the escape from the lunar vicinity in quadrant I or quadrant III in the Sun-B_1 rotating frame with the appropriate energy and eccentricity leads to heliocentric escape. Combining these elements of the disposal problem leads to a useful metric for maneuver planning: the relationship between the phasing of the maneuver itself within the quadrants and heliocentric escape.

For the 9:2 lunar synodic resonant NRHO, a maneuver of 1 m/s in the velocity direction at perilune results in departure from the NRHO after about 40 additional days when navigation and spacecraft errors are not applied to the maneuver, as noted in Table 1 and Figure 17(a). The relationship between maneuver location within the Sun-B_1 rotating frame and heliocentric escape for an error-free 1 m/s maneuver in the velocity direction at perilune on the 9:2 NRHO appears in Figure 24(a). The dataset includes 15 separate reference NRHOs with initial epochs on different dates in May 2023, each with a disposal maneuver placed at every perilune for 50 revolutions, or about a year. Thus, 750 separate disposal maneuvers are represented in Figure 24(a). Changing the number of revolutions in the NRHO prior to the disposal maneuver changes the epoch, and thus the orientation, of the disposal maneuver; the 750 sample disposal maneuvers complete a circle through the quadrants. The points in Figure 24(a) correspond to the location of each disposal maneuver within the quadrants. Maneuvers that lead to escapes are colored red; maneuvers that result in captures are colored blue. From the map of points in Figure 24(a), it is clear that orienting the disposal maneuver in the

center of quadrant II or IV leads to heliocentric escape; a maneuver in quadrant I or III may or may not lead to heliocentric escape. Note that this relationship is only applicable to the 9:2 NRHO with a 1 m/s maneuver in the velocity direction applied at perilune. Changing any of these parameters changes the time to NRHO departure, and thus the relationship between disposal orientation and escape.

A similar analysis is considered for a 15 m/s disposal burn in the velocity direction at perilune along the 9:2 lunar synodic resonant NRHO. The resulting plot appears in Figure 24(b). The higher ΔV results in departure from the NRHO in less than a full revolution, and a maneuver location along a wide band of Sun-Earth orientations leads to heliocentric escape. In general, disposal burns along the Sun-B_1 rotating x-axis is to be avoided in this case.

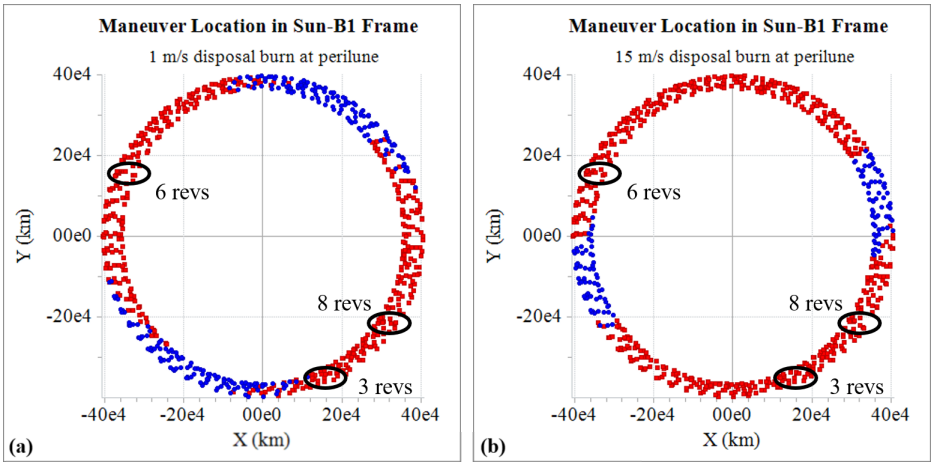

Figure 24: **Disposal maneuver location in the Sun-B_1 rotating frame. Maneuver at perilune of a 9:2 NRHO in the velocity direction, ΔV = 1 m/s (a) and 15 m/s (b). Red maneuvers lead to heliocentric escape; blue maneuvers lead to earthbound trajectories.**

The maps in Figure 24 assume a perfect disposal maneuver. In reality, navigation and maneuver execution errors affect the disposal: recall Figure 17, in which errors applied to the maneuver significantly affect the time to depart the NRHO. The effects of the navigation and maneuver execution errors applied to the disposal burn are explored in a Monte Carlo scenario. Given one selected NRHO reference trajectory, Monte Carlo trials are performed for 6 nominal cases: after 3, 6, or 8 maintained revolutions within the NRHO, a disposal maneuver of 1 m/s or 15 m/s is applied in the velocity direction at perilune. The maneuver locations within the quadrants for each of these disposal maneuvers in the selected reference trajectory are overlaid on the Sun-Earth maneuver orientation plots in Figure 24. All of the maneuver locations lie within the red regions corresponding to escape trajectories. For each case, 500 Monte Carlo trials are run, with navigation and spacecraft errors applied during orbit maintenance and at the time of the disposal maneuver.

The Monte Carlo results are consistent across the cases. For a 1 m/s disposal burn and low navigation errors of 1 km in position and 1 cm/s in velocity (3σ), a disposal maneuver after 8 revolutions results in 495/500 trials achieving heliocentric escape. For maneuvers after both 3 revolutions and 6 revolutions, 499/500 trials successfully achieve heliocentric escape. In Figure 25(a), the time history of the momentum integral appears for each of 500 Monte Carlo trials in one case. The disposal maneuver occurs after 3 maintained revolutions in the NRHO, and after another five post-maneuver orbits near the NRHO, the spacecraft departs the vicinity of the Moon. The heliocentric escapes appear in red; the single earthbound trajectory in blue corresponds to the earliest departure time. Each of the orbits follows a similar pattern, with the navigation and other errors serving to perturb the orbit slightly. The time to depart the NRHO ranges from a minimum of 38.7 days to a maximum of 40.0 days across all trials and cases.

When navigation errors are increased to 10 km in position and 10 cm/s in velocity (3σ), on the other hand, the errors acting on the spacecraft at the disposal maneuver significantly perturb the LM orbit in its post-

disposal trajectory. The time to depart the NRHO varies considerably, from a minimum of 32.9 days to a maximum of 93.1 days, and thus, the solar orientation at NRHO departure is inconsistent. Of 500 trials, only 136 achieve escape to heliocentric space when the disposal burn occurs after 3 maintained revolutions in the NRHO. The time histories of the momentum integral for the 500 trials appear in Figure 25(b), illustrating the varying times of departure from the NRHO. Similarly, escape to heliocentric space is achieved in only 126 and 127 of 500 trials, respectively, for the cases corresponding to disposal burn after 6 and 8 maintained revolutions in the NRHO. Navigation errors of 10 km in position and 10 cm/s in velocity (3σ) at the time of the disposal maneuver lead to unpredictable outcomes for a 1 m/s disposal maneuver applied at perilune.

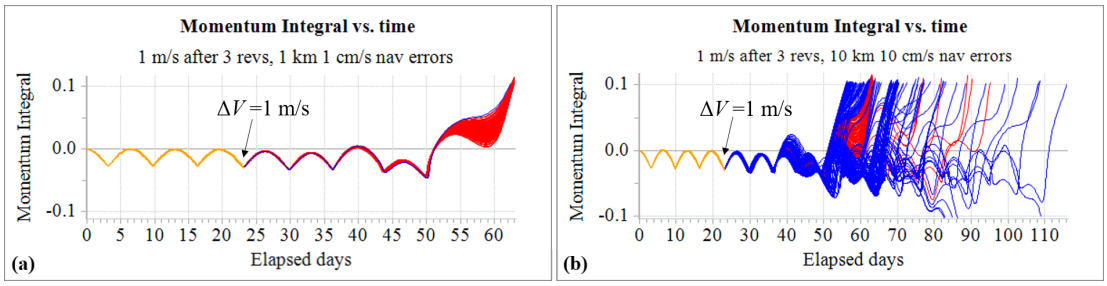

Figure 25: **LM distance from the moon over time after a 1 m/s disposal maneuver following 3 revolutions in the 9:2 lunar synodic resonant NRHO. Low navigation errors (a) and higher navigation errors (b). Red represents heliocentric escape, blue represents earthbound orbits.**

For a maneuver of 15 m/s, on the other hand, the spacecraft departs the vicinity of the Moon after less than a full revolution of the NRHO. The navigation errors thus have less effect on the orientation of the post-NRHO departure trajectory; that is, despite the errors acting on the spacecraft, it still escapes at about the same epoch and orientation. Thus, the errors have much less effect on the success of the Monte Carlo trials. Of the 500 trials run for each of the cases, all successfully escape to heliocentric space. That is, for departure maneuvers of 15 m/s in the velocity direction after 3, 6, or 8 revolutions in the NRHO, with navigation errors up to 10 km in position and 10 cm/s in velocity (3σ), no failures occur. Departure times across all cases range from a minimum of 13.5 days to a maximum of 14.8 days. Sample trajectories representing departure maneuvers of 1 m/s and 15 m/s after 3, 6, and 8 maintained revolutions within the 9:2 NRHO appear in Figure 26. Each sample represents 50 Monte Carlo trials with navigation errors of 1 km and 1 cm/s (3σ) applied during OM and at the disposal maneuver. Disposal burn locations are marked with black arrows. A single failure case is represented when a 1 m/s ΔV is applied after 6 revolutions in the NRHO. Note larger spread in the escaping trajectories in the smaller dV cases.

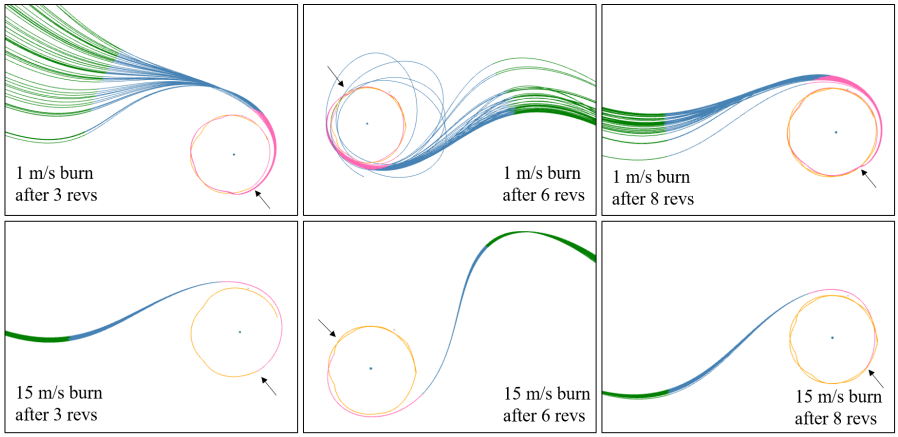

Figure 26: **Six sets of heliocentric escape trajectories in the Sun-B_1 rotating frame. A disposal ΔV is applied after 3, 6, or 8 revolutions in the nominal NRHO.**

CONCLUDING REMARKS

The investigation aims to leverage a bicircular 4-body model to gain better understanding of the escape dynamics in a solar-influenced disposal from an Earth-Moon NRHO. From the analysis in the BCR4BP, multiple factors influencing the disposal are identified. First, the energy along the departure trajectory must be sufficiently high to allow escape through the L_1 or L_2 libration points in the Sun-B_1 system. Second, orienting the departing trajectory appropriately allows the spacecraft to catch the escaping flow and achieve heliocentric escape. Finally, osculating eccentricity along the trajectory must be greater than one, signifying escape from the Earth-Moon vicinity.

Predictions from the BCR4BP effectively describe trajectory behavior in the higher-fidelity force model and are used to generate specific examples of successful Logistics Module disposal scenarios. Successful disposals to heliocentric space are presented for a disposal maneuver magnitude as low as 1 m/s.

ACKNOWLEDGMENT

This work was conducted at NASA Johnson Space Center and Purdue University under contract number NNJ13HA01C with some effort under cooperative agreement NNX13AK60A. The authors thank Ryan Whitley (JSC) and Andrew Cox (Purdue) for useful discussions. Also acknowledged is the Purdue University School of Aeronautics and Astronautics for facilities and support, including access to the Rune and Barbara Eliasen Visualization Laboratory.

REFERENCES

[1] K. Hambleton, "Deep Space Gateway to Open Opportunities for Distant Destinations," `https://www.nasa.gov/feature/deep-space-gateway-to-open-opportunities-for-distant-destinations`, 2017.

[2] C. Warner, "NASA's Lunar Outpost will Extend Human Presence in Deep Space," `https://www.nasa.gov/feature/nasa-s-lunar-outpost-will-extend-human-presence-in-deep-space`, 2018.

[3] G. Gómez, *Dynamics and Mission Design near Libration Points*, Vol. 2. World Scientific, 2001.

[4] J. Guzmán, *Spacecraft Trajectory Design in the context of a Coherent Restricted Four-Body Problem*. PhD Dissertation, Purdue University, West Lafayette, IN, 2001.

[5] M. Andreu, *The Quasi-Bicircular Problem*. PhD Dissertation, Universitat de Barcelona, Barcelona, Spain, 1999.

[6] E. Zimovan, K. Howell, and D. Davis, "Near Rectilinear Halo Orbits and Their Application in Cis-Lunar Space," *3rd IAA Conference on Dynamics and Controls of Space Systems*, Moscow, Russia, 2017.

[7] D. Davis, S. Philips, K. Howell, S. Vutukuri, and B. McCarthy, "Stationkeeping and Transfer Trajectory Design for Spacecraft in Cislunar Space," *AAS/AIAA Astrodynamics Specialist Conference*, Stevenson, Washington, 2017.

[8] S. Vutukuri, "Spacecraft Trajectory Design Techniques Using Resonant Orbits," M.S. Thesis, Purdue University, West Lafayette, Indiana, 2018.

[9] D. Guzzetti, E. Zimovan, K. Howell, and D. Davis, "Near Rectilinear Halo Orbits and Their Application in Cis-Lunar Space," *27th AAS/AIAA Space Flight Mechanics Meeting*, San Antonio, Texas, 2017.

[10] D. Davis, *Multi-body Trajectory Design Strategies Based on Periapsis Poincaré Maps*. PhD Dissertation, Purdue University, West Lafayette, Indiana, 2011.

[11] J. Williams, D. Lee, R. Whitley, K. Bokelmann, D. Davis, and C. Berry, "Targeting Cislunar Near Rectilinear Halo Orbits for Human Space Exploration," *27th AAS/AIAA Space Flight Mechanics Meeting*, San Antonio, Texas, 2017.

[12] C. Newman, D. Davis, R. Whitley, J. Guinn, and M. Ryne, "Stationkeeping, Orbit Determination, and Attitude Control for Spacecraft in Near Rectilinear Halo Orbits," *AAS/AIAA Astrodynamics Specialist Conference*, Snowbird, Utah, 2018.

[13] R. Whitley, D. Davis, M. McGuire, L. Burke, B. McCarthy, R. Power, and K. Howell, "Earth-Moon Near Rectilinear Halo and Butterfly Orbits for Lunar Surface Exploration," *AAS/AIAA Astrodynamics Specialist Conference*, Snowbird, Utah, 2018.

APPENDIX

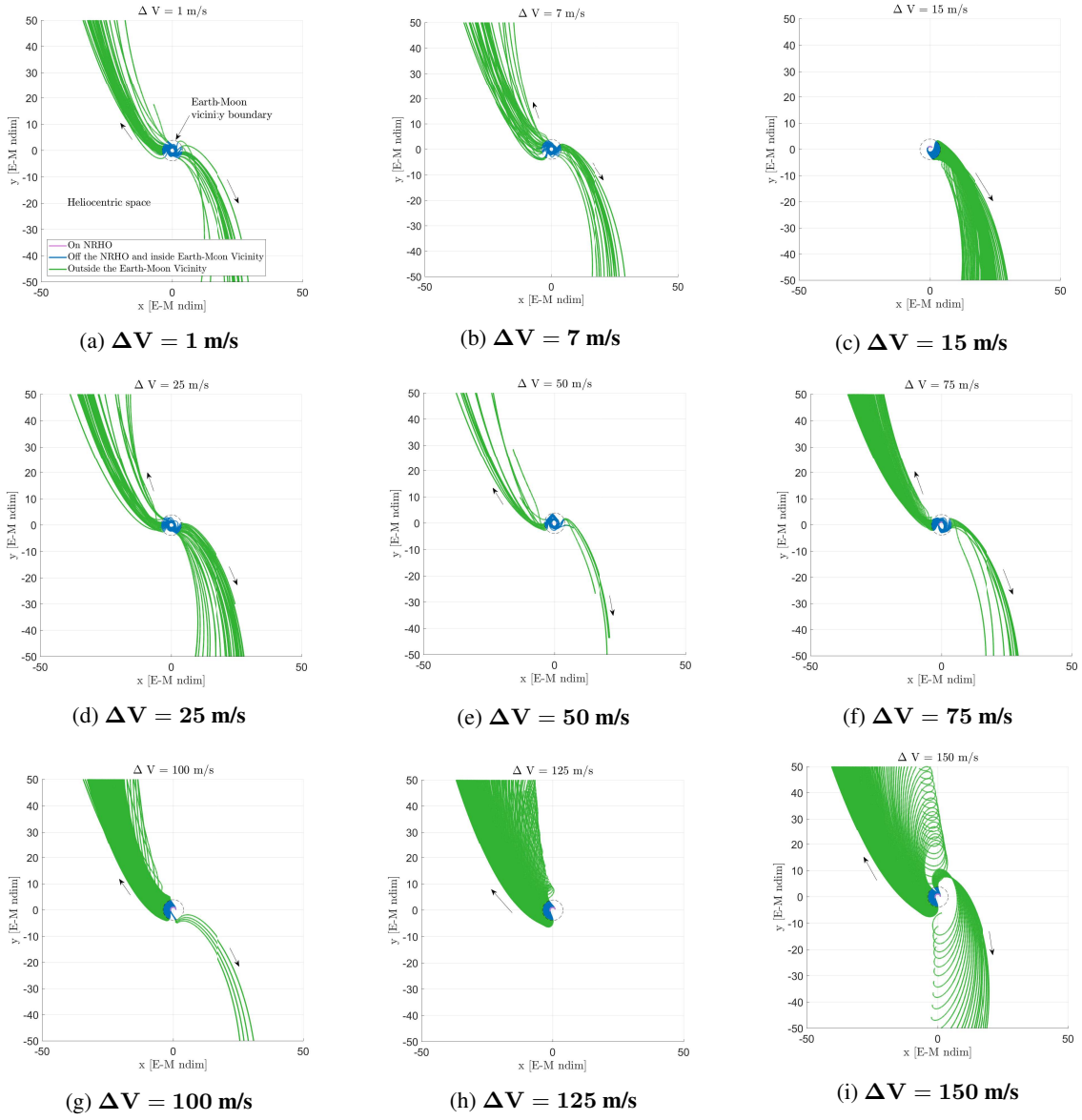

(a) $\mathbf{\Delta V = 1}$ **m/s** (b) $\mathbf{\Delta V = 7}$ **m/s** (c) $\mathbf{\Delta V = 15}$ **m/s**

(d) $\mathbf{\Delta V = 25}$ **m/s** (e) $\mathbf{\Delta V = 50}$ **m/s** (f) $\mathbf{\Delta V = 75}$ **m/s**

(g) $\mathbf{\Delta V = 100}$ **m/s** (h) $\mathbf{\Delta V = 125}$ **m/s** (i) $\mathbf{\Delta V = 150}$ **m/s**

Figure 27: **Indirect and direct escapes trajectories propagated for 365 years for a range of disposal maneuver $\mathbf{\Delta V}$ magnitude, as shown in the Sun-$\mathbf{B_1}$ rotating frame.**

The directions of the departing flow in the Sun-B_1 frame are presented in Figure 27. For a given ΔV magnitude and a range of initial epoch, all the escapes to heliocentric are recorded. The spacecraft either escapes through the left, i.e., through the instantaneous L_1 opening, or through the right, i.e., through the instantaneous L_2 opening. For certain ΔV levels, escapes only occur through L_2 (for instance, Figure 27(c)) while for other magnitudes of the disposal maneuver, all the trajectories are directed toward the Sun, through L_1 (for instance, Figure 27(h)). Note that the higher ΔV levels do not guarantee a better success ratio; more escapes occur at ΔV = 7 m/s (Figure 27(b)) than at ΔV = 50 m/s (Figure 27(e)).

Figure	ΔV [m/s]	Outcome	Time between maneuver and departure from NRHO [days]	Time between maneuver and escape [days]
28	10	Indirect Escape	12.08	165.07
29	7	Capture	16.78	—
30	15	Earth Impact	5.76	—

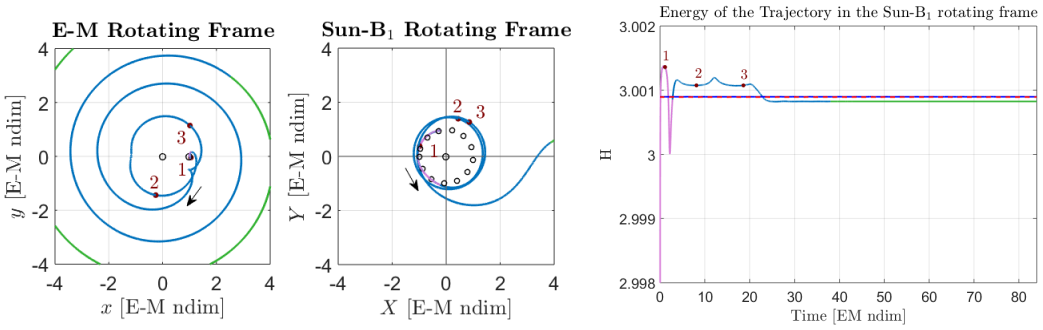

Figure 28: **Indirect Escape (ΔV = 10 m/s)**

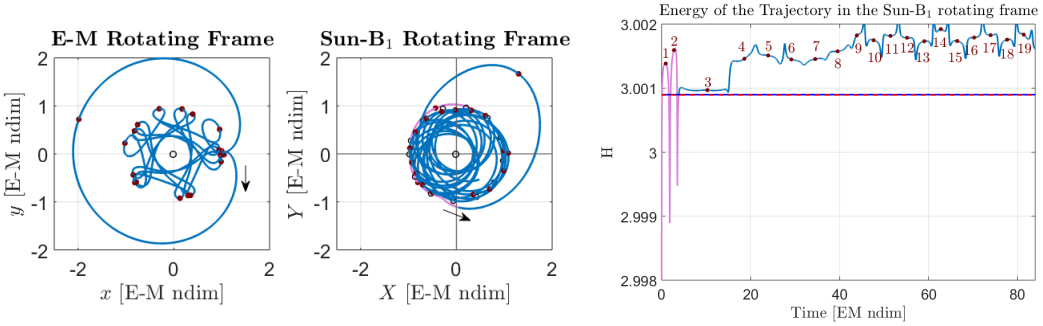

Figure 29: **Capture (ΔV = 7 m/s)**

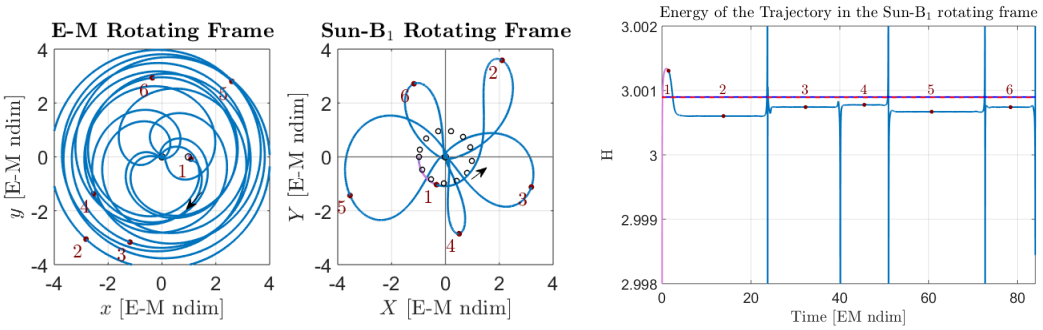

Figure 30: **Earth Impact (ΔV = 15 m/s)**